Journal of
Nanomedicine & Nanotechnology

Shah et al., J Nanomed Nanotechol 2013, 4:3
DOI: 10.4172/2157-7439.1000168

Research Article

Open Access

Enhanced Bioactivity of Ag/ZnO Nanorods-A Comparative Antibacterial Study

A. H. Shah[1], **E. Manikandan**[1]*, **M. Basheer Ahmed**[1] **and V. Ganesan**[2]

[1]*Department of Physics, B.S. Abdur Rahman University, Chennai-600048, India*
[2]*UGC-DAE, CSR, Devi Ahilya University Campus, Devi Ahilya University, Indore-452017, India*

Abstract

Background: In the present work, Ag/ZnO nanorods were synthesized in order to investigate bacterial sensitivity against Gram positive and Gram negative bacteria, comparatively by using well diffusion method.

Materials and methods: Nanoparticles were synthesized by the Sol-Gel method, using $AgNO_3$, $Zn(CH_3CO_2)_2$, NaOH and PVP as capping agent. All the materials were characterized by XRD, HRTEM, PL, FTIR, EDX, and μ-Raman.

Results: The Ag nanoparticles were found attached to crystalline ZnO nanorod. Ag/ZnO nanorods were found to be more effective towards Gram positive, and thus contribute to the greater mechanical damage to all functions of bacteria and enhanced bactericidal impact of Ag on ZnO nanoparticles.

Conclusions: Sol-Gel method was found to be an effective chemical method to synthesis Ag/ZnO metal-semiconductor nanorods. ZnO was found to be good match for Ag, for enhanced and synergistic antibacterial activities, for both Gram positive and Gram negative bacteria. So, this study provided both theoretical and experimental support for the practical applications of Ag/ZnO nanorods.

Keywords: Nano ZnO; Silver; Sol-gel; Antibacterial study; Well diffusion

Introduction

Semiconductor oxides with noble or transition, or rare earth metal nanocomposites are interesting because of their superior optical, electrical, magnetic and chemical properties. These properties that arise from their combination, deliver the materials interesting in different application areas, including nanoelectronics devices, catalysis, nonlinear optical devices, bio-medical, etc [1-3]. In these nanocomposites, materials with different properties can be grouped in same particle to perform multiple technological functions. However, they can also show new properties and functionalities due to the strong interaction between the two different functional components [4,5]. Metal-oxides semiconductor nanocomposites have been extensively explored because of their potential applications in wide fields. Among them, Ag/ZnO nanocomposites have attracted large attention, not only because ZnO is one of the most important wide-band gap semiconductors and has various applications, including use in sensors, electronics, solar cells and photo electronics, but also because silver nanomaterials display some unique features in chemical and biological sensing, which are based on surface-enhanced Raman scattering (SERS), localized surface plasmon resonance (SPR), and metal-enhanced fluorescence [6]. In addition, silver modification is found to be effective for the fabrication of p-type ZnO, as the naturally occurring ZnO displays n-type conductivity due to its native defects such as zinc interstitials and oxygen vacancies [7]. In recent years, silver ions become more interests of the several research works, because of their novel effects on the efficiency of photoactivity of semiconductor photocatalysis and their evolution on antibacterial activity [8]. On the other hand, ZnO has received much attention over the past few decades because it has a wide range of properties that depend on doping, including a range of conductivity from metallic to insulating (including *n*-type and *p*-type conductivity), high transparency, piezoelectricity, wide-band gap (3.37 eV at 300 K), large binding energy (60 meV), high melting point ~1975C, semi-conductivity, room-temperature ferromagnetism, and huge magneto-optic and chemical-sensing effects [8-10]. Without much effort, it can be grown in many different nanoscale forms, thus allowing different novel devices to be achieved. Many efforts have been made alone to synthesize ZnO with various morphologies in the nanoregime, including rods [11], belts [12], prisms [13], wires [14], rings [15], flowers [16], and many more. Various techniques that have been used to synthesize Ag/ZnO composites include template-confined synthesis routes [17], high-temperature methods [18], hydrothermal synthesis [19], solution-phase methods using additives, such as surfactants [20], sonochemical method and microwave heating [21]. In the present article, we report on the synthesis of Ag/ZnO nanorods of the order of 100 nm diameters through facile chemical sol-gel method. Effects of incorporation of Ag into ZnO crystal on their optical, structural and antibacterial behavior of the ZnO nanorods are studied in details.

Experimental Techniques

Sample synthesis

All the chemical reagents were of analytical grade and used without further purification in this experiment.

Synthesis of undoped and doped ZnO nanorods: High purity zinc acetate [$Zn(CH_3CO_2)_2$], silver nitrate $Ag(NO_3)_2$, sodium hydroxide

***Corresponding authors:** Manikandan E, Department of Physics, B.S. Abdur Rahman University, Chennai-600048, India, E-mail: mani@bsauniv.ac.in

Basheer Ahmed M, Department of Physics, B.S. Abdur Rahman University, Chennai-600048, India, E-mail: basheerahamed@bsauniv.ac.in

Received February 02, 2013; **Accepted** March 01, 2013; **Published** March 04, 2013

Citation: Shah AH, Manikandan E, Ahmed MB, Ganesan V (2013) Enhanced Bioactivity of Ag/ZnO Nanorods-A Comparative Antibacterial Study. J Nanomed Nanotechol 4: 168. doi:10.4172/2157-7439.1000168

(NaOH) and poly vinylpyrrolidone (PVP) as capping agent, were used for chemical processing. In a typical procedure for the synthesis of pure ZnO, 0.05 M zinc acetate was dissolved in 100 ml of de-ionized water and 0.1 M NaOH was dissolved in 100 ml deionized water. NaOH solution was added drop wise to zinc acetate solution. Then, a white colored gel is produced and this gel was kept for ageing overnight. Similarly for the synthesis of Ag doped ZnO nanorods, 0.1 M zinc acetate $Zn(Ac)_2$ solution with milimolar silver nitrate and aqueous ammonia (1:1) was added drop wise to reach a pH ~ 7, and the stirring was continued for another 30 minutes. A few drops of PVP were also added during stirring for controlling growth. The formed glassy like white gel was allowed to age overnight. It was filtered, washed, dried at 100°C for 12 hrs and annealed at 500°C for 2 hrs in a muffle furnace, fitted with a proportional-integral-derivative (PID) temperature controller, and the heating rate was set at 100°C per minute.

Characterization: The synthesized doped and Ag doped ZnO nanorods were characterized by XRD with nickel-filtered CuKα radiation source (λ=1.5417 Å, 2θ range 5-80° and 0.02 step size) for the crystallinity, phase purity and average particle crystallites size. The surface morphology and microstructure was investigated by high resolution HRTEM; Tecnai F20. The compositional analysis of synthesized samples was carried out using energy-dispersive EDX. The optical emission spectra was measured by an F-2500 spectrophotometer, with Xe900 (450 W xenon arc lamp) as the excitation source, with a spectral slit width of 1 nm in back scattering configuration. A confocal micro-Raman study excited by the 488 nm line of Ar^+ laser (power 100 W) was used for synthesized samples. The scanning speed and step for measurements were 60 nm/min and 0.5 nm, respectively. All the spectra and characterization were observed at RT.

Antibacterial test: Well diffusion method was used to determine the antibacterial activity of the Gram negative bacteria, *V. cholera,* towards pure undoped and doped ZnO nanorods. This bacterium is an Asian bacterium, and is related to cholera infections which are most commonly acquired from drinking water in which this bacteria is found naturally, or into which it has been introduced from the feces of an infected person. Well diffusion is a very cost-effective, facile and useful method for assessing the antibacterial properties. In this method, sterile nutrient agar plate was prepared and these agars are poured into the sterilized Petri dish. The 100 µl of cultured bacterial cell suspension were spread over the agar plate using sterile glass rod. The plates were allowed for 1 min to dry and sterile well cutter of diameter 9 mm was used to bore wells in the agar plates. Subsequently, a 100 µl of the nanoparticle suspension was introduced into wells of the inoculated nutrient gar plates. The plates were allowed to stand for 1 h or more for diffusion to take place, and then incubated at 37°C for 24 h and the diameter of inhibitory zones was measured in millimeter (mm).

Results and Discussions

Structural studies

The change of crystalline phase structure of Ag/ZnO composite were investigated by XRD at room temperature (RT). Figure 1a shows the XRD pattern of uncoated ZnO nanoparticles recorded in the range of 20° to 80°, with a scanning step size 0.02°. All diffraction peaks attributed to crystalline of ZnO with the hexagonal wurtzite structure (space group: P63mc (186); a=0.325 nm, c=0.519 nm). The data obtained are in good agreement with the joint committee on powder diffraction standards (JCPDS) card for ZnO (JCPDS 036-1451). The strongest peaks were detected at 2θ values are: 31.7°, 34.4°, 36.17°, 47.5°, 56.6°, 62.2°, 66.4°, 68° and 69.1°, corresponding to the following lattice (hkl) planes: (100), (002), (101), (102), (110),(103), (200), (112), and (201), respectively. Two additional weak peaks are obtained at 38.18° and 44.36°, as shown in figure 1b, which can be assigned to the (111) and (200) crystal planes of face centered cubic (fcc) structure of Ag crystalline (JCPDS 4-0783) [22]. These peaks are weak presented due to their low content. The average particle grain size (D) can be calculated from the width of lines in the XRD spectrum, with the aid of Scherrer formula [23]. The calculated D values of Ag nanoparticles estimated around 10 nm, and that of ZnO nanorods were found to be decreased from 17 nm to 12 nm after Ag coating.

Morphological and compositional studies

In order to obtain the information about Ag distribution in the as-synthesized samples, HRTEM observations and EDX mapping measurements were carried out, as shown in figure 2. A typical HRTEM image of an individual Ag/ZnO composite sample, as shown in figure 2a, reveals that metallic Ag nanoparticle attaches on the surface of ZnO nanorod. The composition of the as-synthesized is further characterized by EDX, and the results are shown in figure 2b. Almost all the peaks on the curves are ascribed to Zn, Ag and O elements and some additional ones. These additional peaks may be belong to Cu and C elements are form sampler holder with conductive tap. Thus, it is concluded that the as-synthesized samples are composed of Zn, Ag and O elements, which is in good agreement with XRD and FTIR.

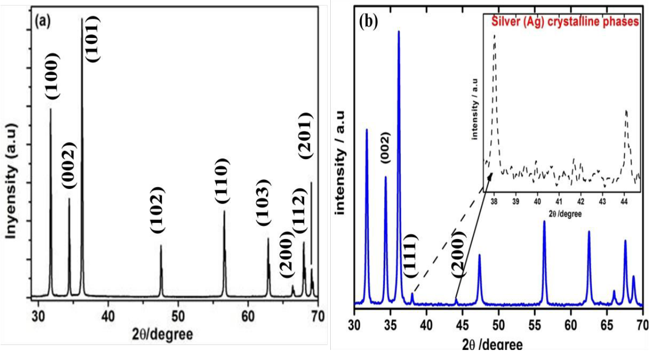

Figure 1: X-ray diffractions pattern of a) uncoated ZnO and b) Ag-ZnO nanorods.

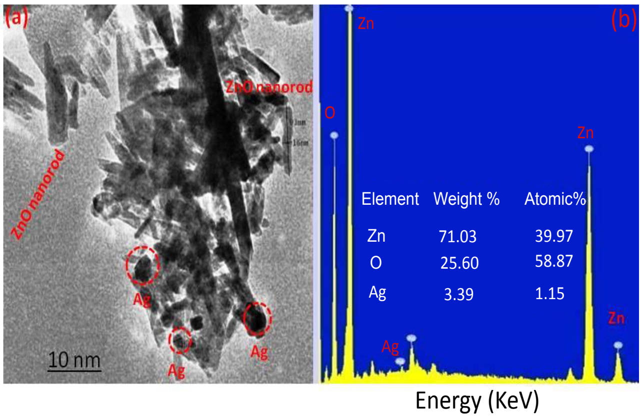

Element	Weight %	Atomic%
Zn	71.03	39.97
O	25.60	58.87
Ag	3.39	1.15

Figure 2: (a) HR-TEM images of Ag attached with ZnO nanorods (b) EDAX.

Optical study

The room temperature PL spectra (excitation at 325 nm) of pure and doped ZnO nanoparticles are shown in figure 3. It is used to verify the quality crystal and possible effects of Ag coating on ZnO nanostructures. Generally, the PL spectrum of ZnO consists of UV emission and the visible broadband emission [24]. The UV-range emission, called radioactive recombination, occurs due to the recombination between the electrons in a conduction band and the holes in a valence band. On the other hand, the visible range emission, called nonradioactive recombination, occurs due to the recombination between the electrons in a deep defect level or a shallow surface defect level, and the holes in a valence band [25,26]. Therefore, in case of both samples shown in figures 2a and b, the narrow UV emission band centered at around 359 and 334 nm is ascribed to the radiative recombination. It could be seen from PL spectra that the UV emission in Ag/ZnO composite is decreasing due to the distinct surface plasmon resonance (SPR) effect of noble metals, Ag or Au, indicating the decrease in electron-hole recombination. This decrease in emission intensity is in accordance with the Stern-Volmer quenching, and similar results were previously reported [27]. Further in pure ZnO PL spectrum, the two weak blue bands obtained at 417 and 438 nm are corresponding to band edge free excitons and bound excitons, respectively [28]. Furthermore, there is a green emission observed at ~ 547 nm, was often attributed to singly ionized oxygen vacancies (V_O^+) [29], while other reports indicated the green emission (~ 521 nm) was due to oxide antisite defect (O_{Zn}) [30]. Moreover, the green emission (~ 520 nm) of ZnO nanostructures was also attributed to oxygen vacancies and zinc interstitials (Zn_i) [31]. After Ag coating effect of the PL, emission peaks increased in the order of UV to visible regime as 334,390,423,469 and 570 nm, shown in the spectral lines. The additional peak, 390 nm, was found in the samples usually called near band edge (NBE), which is attributed to excitonic recombination. The peaks, 423 and 469 nm, got red shifted from 417 and 438 nm (Figure 3a and b). This shift is attributed to shape changes of particles. Actually, the peak positions of PL spectra are significantly dependent on the size of the ZnO crystalline due to the quantum-confinement effect, which will induce gap enhancement [32]. The size of ZnO nanoparticles decreases from 57 nm to 52 nm in our case. So, the red-shift for UV emission may be related to the quantum-confinement effect of the ZnO nanoparticles. The effects of defects or/and impurities due to Ag doping on PL, can be observed by the FWHM measurement of free exciton emission. Generally, FWHM of intrinsic emission in PL spectrum is related to the crystal quality. A small FWHM indicates that the crystal is of high quality, and its large value suggests the crystal is imperfect, showing it may have point defects. Meanwhile, FWHM the values for both samples are nearly close to each other. These results indicate Ag coating does not effectively degrade the crystal.

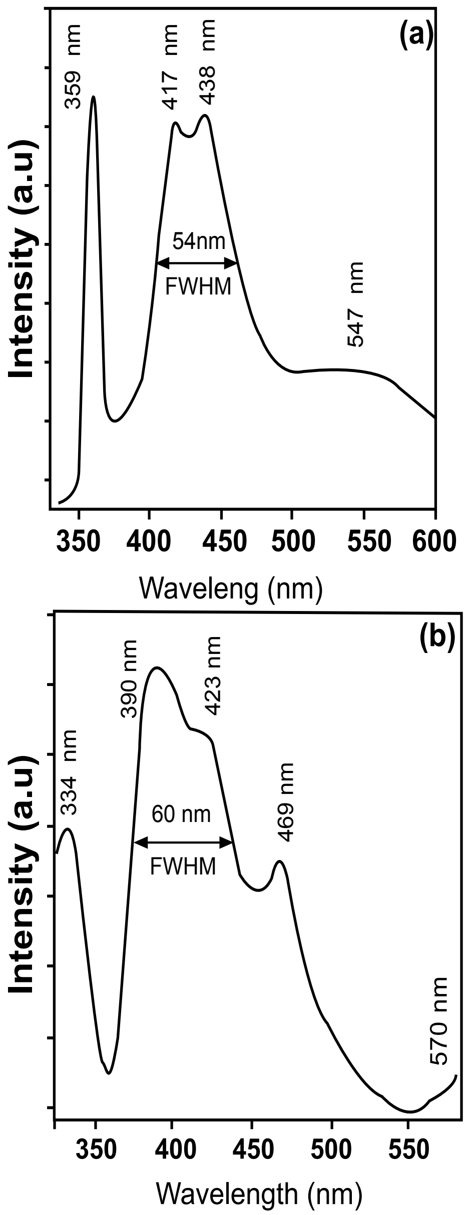

Figure 3: PL spectra of (a) ZnO (b) Ag-ZnO nanorod.

Micro-Raman (μ-RS) scattering study

To investigate the influence of Ag on the molecular vibrational modes of ZnO nanoparticles, room temperature Raman spectra of ZnO and Ag-nanorods in the spectral range of 200 to 800 cm^{-1} were measured, as shown in figure 4. According to group theory, the structure of ZnO belongs to the C_{6V} symmetry group, which predicts two A_1, two E_1, two E_2 and two B_1 modes. Among these, A_1 and E_1 modes are polar, and split into transverse (TO) and longitudinal optical (LO) phonons, all being Raman and infrared active. E_2 modes are only Raman active, and B_1 modes are infrared, and Raman inactive (silent modes). The Raman spectra of undoped ZnO nanoparticles consist of peaks that were observed at 331 cm^{-1} (second-order vibration), 380, 409, 438, 537, 581, 658, and 720 cm^{-1}, corresponding to the E_{2H}-E_{2L}, A_1(TO), E_1 (TO), E_{2H}, TO+TA(M), E_1 (LO) and E_{2L}-B_{1H} fundamental phonon modes of hexagonal ZnO, respectively [33-37]. The 331 cm^{-1} mode could be observed by enhancement of Raman active and inactive phonons, with lattice symmetry due to disorder-activated Raman scattering (DARS) [38,39]. The 380 cm^{-1} mode was lifted the degeneracy of infrared active optical phonons into a transverse (TO) branch, as is well known by the Lyddane–Sachs–Teller relation [40]. The 409 cm^{-1} mode is associated with lattice disorder along the c-axis of the ZnO crystal, the 438 cm^{-1} mode corresponds to E_2 mode of wurtzite ZnO, and a very sharp feature. The 582 cm^{-1} E_1 (LO) corresponds to well resolve Raman peaks due to multiphonon and resonance processes, and are related to oxygen deficiency. According to the reports of Li et al. [39], the 537 cm^{-1} peak is a Zn–C mode, and the 658 cm^{-1} peak was a Zn–CH_2 mode, which

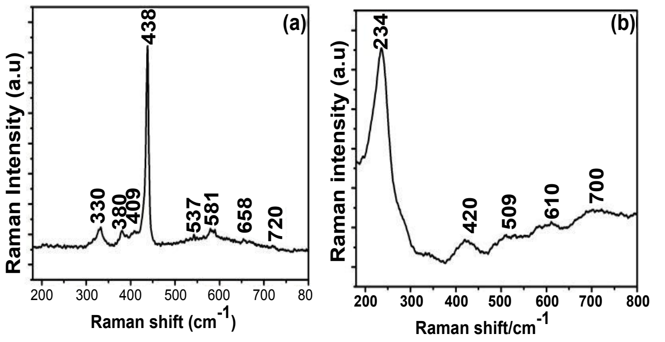

Figure 4: Micro-Raman scattering of (a) pure ZnO (b) Ag-ZnO.

are associated with the precursor materials in the sol-gel process. Ag/ZnO composite related vibrational modes were identified as follows: 234, 343, 420, 509, 610, and 700 cm^{-1}. The additional peak at 234 cm^{-1} obtained in the given spectrum is due to the radial effect of Ag atoms. The main peak, 438 cm^{-1}, slightly red shifted to lower wavenumber of 420 cm^{-1}, with the increment of 2 cm^{-1}. Respectively, the PL studies confirmed the red shift of 20 nm in the doped materials; this might be confirming the size effect of quantum confinement.

Molecular vibrational study

The FTIR spectrum of ZnO and Ag/ZnO nanostructures were recorded in the range 400-4000 cm^{-1}, using FTIR spectrometer, is given in figure 5. From the FTIR spectrum, various functional groups and metal-oxide (MO) bond present in the compound were analyzed. In the FTIR spectrum, a significant band at ~ 475 and 425 cm^{-1} is assigned to the characteristic stretching mode of Ag-O and Zn-O bond [41-43]. The peak at ~ 940 cm^{-1} may be attributed to aromatic C=C stretching mode [44]. Absorption band at ~ 3425 cm^{-1} arises due to the stretching mode of O-H group, that reveals the existence of a small amount of water absorbed by the ZnO nanostructure [45,46]. The peak located at ~ 2344 cm^{-1} is due to atmospheric CO_2 present in the instrument. Stretching modes of C-O and C=O are observed at ~ 1387.31 cm^{-1} and 1533.86 cm^{-1}. On doping, stronger and wider absorption bands are observed in the region ~ 1170-878 cm^{-1} due to the organic capping of nano silver.

Antibacterial studies

In our study, the relative antibacterial activity of ZnO and Ag/ZnO suspensions of particles of different sizes around 17 nm and 12 nm towards Gram positive (*M. leutus*) and Gram negative (*K. pneumonia*) bacteria were studied in aqueous in LB broth (Figure 6). The well diffusion method is used to test the ability of the antibacterial agent to rupture the bacterial cells, and inverse relationship has been found between the particle size and its activity. The reason may be due to the increase in the surface-to-volume ratio of small size particles, and hence, a greater penetrating ability and reactivity [47]. At the concentration of 1 mg/ml, the antibacterial activity studied against Gram negative and positive bacteria, as shown in figure 5. The observed mean inhibition zones for ZnO are around 14 and 18 mm and for Ag/ ZnO nanorods, these values increased to 19 and 23 mm, respectively against given bacteria mentioned in the table 1. From these zone measurements, it could be stated that Ag/ZnO composite possesses effective antibacterial property, when compared to ZnO nanoparticle. The antibacterial activity of nanoparticles can may either directly interact with the microbial cells (e.g. interrupting trans membrane electron transfer, disrupting/penetrating the cell envelope and oxidizing cell components), or produce secondary products (e.g. reactive oxygen species (ROS)) that cause damage. Only a few reports are available in the case of antibacterial properties of doped ZnO. There are numerous mechanisms behind the antibacterial activity of MOs. More recently, Padmavathy and Vijayaraghavan [48] reported that ZnO is activated by white lights to increase electron-hole pairs. These holes split the H_2O molecule from the suspension of ZnO into hydroxyl radical (OH^-) and hydrogen ion (H^+). Dissolved oxygen molecules are converted to superoxide radical anions (O_2^-), which react with hydrogen ion (H^+), to produce HO_2^- radical. These hydroxyl radicals on collision with electrons produce hydrogen peroxide anions HO_2, which react with hydrogen to produce H_2O_2 molecules. These generated H_2O_2 molecules can penetrate the cell membrane and kill the bacteria. The hydroxyl radicals OH^- and O_2^-, super oxide radical anion are negatively charged particles, they cannot penetrate into the cell membrane and must remain in contact with outer surface of the bacteria, and however,

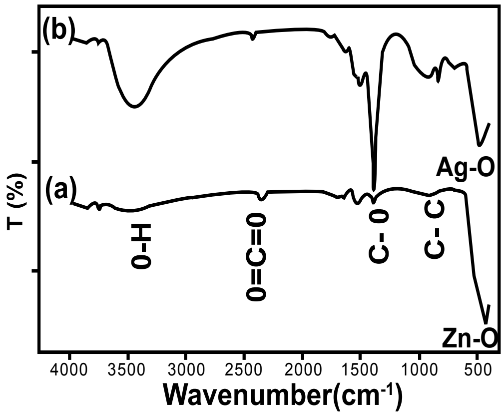

Figure 5: FTIR spectra of (a) ZnO (b) Ag-ZnO nanorods.

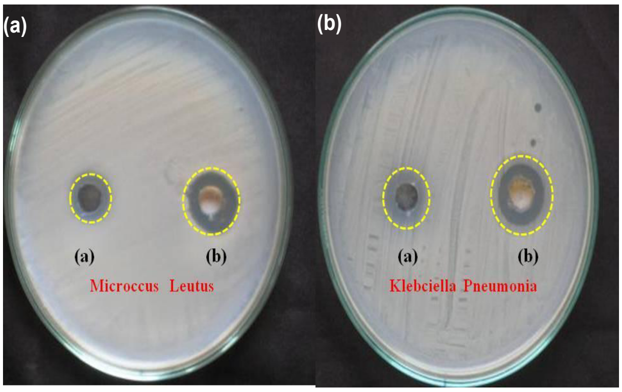

Figure 6: Antibacterial test for inhibition zones of (a) ZnO (b) Ag-ZnO nanorods *M. leutus* and *K. pneumonia* bacteria.

Bacterial culture	Inhibition Zones (nm)	
	ZnO	Ag/ZnO
M. leutus	14	19
K. pneumonia	18	23
Grain Size (nm)	17	12

Table 1: Inhibition Zones of ZnO and Ag/ZnO nanorods against *M. leutus* and *K. pneumonia.*

H_2O_2 penetrate into the cell [49]. These active molecules are effectively toxic to bacterial substances. In addition, the damage of cell membrane might directly lead to the leakage of minerals, proteins and genetic materials, causing ultimate cell death. Another mechanism behind the cell envelope is ZnO, which can produce the Zn^{2+} ions [50-52]. These ions penetrate into the interior cell first. The physical contact between the cell membrane and ZnO could also be observed because of the electrostatic force of attraction. But, physical contact is being the main reason for the bacterial toxicity of the microorganism. By inducing the chemical reaction between the bacterial cultures and nanoparticles, an effective antibacterial activity could be observed. As a result, the creation of active species from the nanoparticles will directly influence the cellular inhibition. From antibacterial test, we confirmed that Ag/ZnO nanoparticles render an effective antibacterial agent, when compared to pure ZnO. It was also interesting to note that both the samples had strong antibacterial activity against both Gram negative and positive bacterial culture. Therefore, it could be concluded that the creation of active species by photo induced reaction are the main source towards the bacterial toxicity, in the case of metal transition metal oxides (TCMO) compounds.

Conclusion

Ag/ZnO nanorods were synthesized by the simple wet chemical sol-gel method. The grain size was controlled by using polyvinyl pyridine as capping agent. Nanoparticle crystallinity, quality of the samples, chemical composition, and the optical properties were investigated by XRD, μ-RS, FTIR, PL spectrometer and HR-TEM. The enhanced bioactivity was demonstrated by studying the antibacterial activity of ZnO and Ag/ZnO samples. These improved bioactivities of smaller particles were attributed to the higher surface to volume ratio. The smaller particles need more particles to cover a bacterial colony, which results in the generation of active oxygen species, which will kill bacteria more effectively. Therefore, Ag/ZnO nanorods were found to be more effective towards Gram negative and thus, contribute to the greater mechanical damage for all the functions of bacteria, and enhanced bactericidal impact of uniform fine structured Ag/ZnO nanorods.

Acknowledgments

One of the author, Mr. A.H. Shah would like to thank Dr. Vasant Sathe, IUC-DAE consortium for Scientific Research (CSR), Indore for Micro-Raman Scattering study.

References

1. Shah AH, Baheer Ahamed M, Manikandan E, Iydroose M (2013) Magnetic, optical and structural studies on Ag doped ZnO nanoparticles. J Mater Sci: Mater Electron.
2. Manikandan E, Moodley MK, Sinha Ray S, Panigrahi BK, Krishnan R, et al. (2010) Zinc oxide epitaxial thin film deposited over carbon on various substrate by pulsed laser deposition technique. J Nanosci Nanotechnol 10: 5602-5611.
3. Liu X, Afzaal M, Ramasamy K, O'Brien P, Akhtar J (2009) Synthesis of ZnO hexagonal single-crystal slices with predominant (0001) and (0001) facets by poly(ethylene glycol)-assisted chemical bath deposition. J Am Chem Soc 131: 15106-15107.
4. Fie L, Wu J, Qin Q, Li Z, Huang X (2010) A facile method to prepare monodispersed ZnO–Ag core-shell microspheres. Superlattices Microstruct 47: 232-240.
5. Fie L, Yuan Y, Luo J, Qin Q, Wu J, et al. (2010) Synthesis and characterization of ZnO–Ag core-shell nanocomposites with uniform thin silver layers. Appl Surf Sci 256: 6076-6082.
6. Ye XY, Zhou YM, Sun YQ, Chen J, Wang ZQ (2009) Preparation and characterization of Ag/ZnO composites via a simple hydrothermal route. J Nanopart Res 11: 1159-1166.
7. Georgekutty R, Seery MK, Pillai SC (2008) A highly efficient Ag-ZnO photocatalyst: synthesis, properties, and mechanism. J Phys Chem C 112: 13563-13570.
8. Vaidyanathan R, Kalishwaralal K, Gopalram S, Gurunathan S (2009) Nanosilver--the burgeoning therapeutic molecule and its green synthesis. Biotechnol Adv 27: 924-937.
9. Zhang L, Jiang Y, Ding Y, Daskalakis N, Ding Y, et al. (2010) Mechanistic investigation into antibacterial behavior of suspensions of ZnO nanoparticles against *E. coli.* Nanopart Res 12: 1625-1636.
10. Karunakaran C, Rajeshwari V, Gomathisankar P (2011) Combustion synthesis of ZnO and Ag–doped ZnO and their bactericidal and photocatalytic activities. Superlattices Microstruct 50: 234-241.
11. Li Z, Xiong Y, Xie Y (2003) Selected-control synthesis of ZnO nanowires and nanorods via a PEG-assisted route. Inorg Chem 42: 8105-8109.
12. Wang X, Ding Y, Li Z, Song J, Wang ZL (2009) Single-crystal mesoporous ZnO thin films composed of nanowalls. J Phys Chem C 113: 1791-1794.
13. Wang D, Song C (2005) Controllable synthesis of ZnO nanorod and prism arrays in a large area. J Phys Chem B 109: 12697-12700.
14. Huang MH, Mao S, Feick H, Yan H, Wu Y, et al. (2001) Room-temperature ultraviolet nanowire nanolasers. Science 292: 1897-1899.
15. Liu B, Yu SH, Zhang F, Li L, Zhang Q, et al. (2004) Ring-Like nanosheets standing on spindle-like rods: Unusual ZnO superstructures synthesized from a flakelike precursor $Zn_5(OH)_8Cl_2$. H_2O. J Phys Chem B 108: 4338-4341.
16. Peng Y, Xu AW, Deng B, Antonietti M, Cölfen H (2006) Polymer-controlled crystallization of zinc oxide hexagonal nanorings and disks. J Phys Chem B 110: 2988-2993.
17. Zhang H, Ma XY, Xu J, Niu JJ, Yang D (2003) Arrays of ZnO nanowires fabricated by a simple chemical solution route. Nanotechnology 14: 423-428.
18. Wang Z, Qian XF, Yin J, Zhu ZK (2004) Large-scale fabrication of tower-like, flower-like, and tube-like ZnO arrays by a simple chemical solution route. Langmuir 20: 3441-3448.
19. Aneesh PM, Vanaja KA, Jayaraj MK (2007) Synthesis of ZnO nanoparticles by hydrothermal method. Nanophotonic materials IV 6639: 66390J.
20. Oliveira APA, Hochepied JF, Grillon F, Berger MH (2003) Controlled precipitation of ZnO particles at room temperature. Chem Mater 15: 3202-3207.
21. Kowsari E (2011) Sonochemically assisted synthesis and application of hollow spheres, hollow prism, and coralline-like ZnO nano photocatalyst. J Nanopart Res 13: 3363-3376.
22. Zheng Y, Zheng L, Zhan Y, Lin X, Zheng Q, et al. (2007) Ag/ZnO heterostructure nanocrystals: synthesis, characterization, and photocatalysis. Inorg Chem 46: 6980-6986.
23. Srinivasan G, Kumar RR, Kumar J (2007) Li doped and undoped ZnO nanocrystalline thin films: a comparative study of structural and optical properties. Journal of Sol-Gel Science and Technology 43: 171-177.
24. Ghosh A, Deshpande NG, Gudage YG, Joshi RA, Sagade AA, et al. (2009) Effect of annealing on structural and optical properties of ZnO thin film deposited by successive ionic layer adsorption and reaction technique. J Alloys Compd 469: 56-60.
25. Yguerabide J, Yguerabide EE (1988) Light-scattering submicroscopic particles as highly fluorescent analogs and their use as tracer labels in clinical and biological applications. Anal Biochem 262: 137-156.
26. Vanheusden K, Waren WL, Seager CH, Tallant DR, Voigt J A, et al. (1996) Mechanisms behind green photoluminescence in ZnO phosphor powders. J App Phys 79: 7983-7991.
27. Subramanian V, Wolf EE, Kammat PV (2003) Green emission to probe photoinduced charging events in ZnO–Au nanoparticles charge distribution and fermi-level equilibration. Phys Chem B 107: 7479-7485.
28. Wu XL, Siu GG, Fu CL, Ong HC (2001) Photoluminescence and cathodoluminescence studies of stoichiometric and oxygen-deficient ZnO films. Appl Phys Lett 78: 2285-2287.
29. Yang Q, Tang K, Zuo J, Qian Y (2004) Synthesis and luminescent property of single-crystal ZnO nanobelts by a simple low temperature evaporation route. Appl Phys A 79: 1847-1851.

30. Lin B, Fu Z, Jia Y (2001) Green luminescent center in undoped zinc oxide films deposited on silicon substrates. Appl Phys Lett 79: 943-945.
31. Yang N, Yang H, Qu Y, Fan Y, Chang L, et al. (2006) Preparation of Cu–Zn/ZnO core–shell nanocomposites by surface modification and precipitation process in aqueous solution and its photoluminescence properties. Mater Res Bull 41: 2154-2160.
32. Changle W, Shen L, Huaguang Y, Qingli H, Zhang YC (2011) Synthesis of Sn-doped ZnO nanorods and their photocatalytic properties. Mater Res Bull 46: 1107-1112.
33. Pal U, Serrano JG, Santiago P, Xiong G, Ucer KB, et al. (2006) Synthesis and optical properties of ZnO nanostructures with different morphologies. Opt Mater 29: 65-69.
34. Music S, Dragcevic D, Popovic S, Ivanda M (2005) Precipitation of ZnO particles and their properties. Mater Lett 59: 2388-2393.
35. Xing YJ, Xi ZH, Xue ZQ, Zhang XD, Song JH, et al. (2003) Optical properties of the ZnO nanotubes synthesized via vapor phase growth. Appl Phys Lett 83: 1689-1692.
36. Manouni AE, Manjo FJ, Mollar M, Mari B, Gomez R, et al. (2006) Effect of thermal annealing on ZnO: Al thin films grown by spray pyrolysis. Superlattices Microstruct 39: 134-139.
37. Manjon FJ, Mari B, Serrano J, Romero AH (2005) Silent Raman modes in zinc oxide and related nitrides. J Appl Phys 97: 53516-53519.
38. Mead DG, Wilkinson GR (1977) The temperature dependence of the raman effect in some wurtzite type crystals. J Raman Spectrosc 6: 123-129.
39. Li BB, Xiu XQ, Zhang R, Xie ZL, Chen Y, et al. (2004) Structure and magnetic properties of Co-doped ZnO Powder prepared by sol-gel method. 13th International Conference on Semiconducting and Insulating Materials 202-205.
40. Serrano J, Romero AH, Manjon FJ, Lauck R, Cardona M, et al. (2004) Pressure dependence of the lattice dynamics of ZnO: An *ab initio* approach. Phys Rev B 69: 94306-94314.
41. Wahab R, Ansari SG, Kim YS, Seo HK, Kim GS, et al. (2007) Low temperature solution synthesis and characterization of ZnO nano-flowers. Mater Res Bull 42: 1640-1648.
42. Gupta TK, Hower PL (1992) A barrier model for ZnO varistors. J App Phys 50: 4847-4856.
43. Parvin T, Keerthiraj N, Ibrahim IA, Phanichphant S, Byrappa K (2012) Photocatalytic degradation of Municipal wastewater and brilliant blue dye using hydrothermally synthesized surface-modified silver-doped ZnO designer particles. International Journal of Photoenergy 67: 610-618.
44. Gayen RN, Sarkar K, Hussain S, Bhar R, Pal AK (2011) ZnO films prepared by modified sol-gel technique. Indian Journal of Pure and Applied Physics 49: 470-477.
45. Nakamoto K (1997) Infrared spectra of inorganic and coordination compounds. (2nd Edn), Wiley, New York, USA.
46. Cao H, Zhao YG, Ong HC, Ho ST, Dai J Y, et al. (1998) Ultraviolet lasing in resonators formed by Scattering in semiconductor polycrystalline films. Appl Phys Lett 73: 3656-3658.
47. Dutta RK, Sharma PK, Bhargava R, Kumar N, Pandey AC (2010) Differential susceptibility of Escherichia coli cells toward transition metal-doped and matrix-embedded ZnO nanoparticles. J Phys Chem B 114: 5594-5599.
48. Padmavathy N, Vijayaraghavan R (2008) Enhanced bioactivity of ZnO nanoparticles-an antimicrobial study. Sci Technol Adv Mater 9: 432-438.
49. Tam KH, Djurisic AB, Chan CMN, Xi YY, Tse CW, et al. (2008) Antibacterial activity of ZnO nanorods prepared by hydrothermal method. Thin Solid Films 516: 6167-6174.
50. Karunakaran C, Rajeshwari, Gomathisankar P (2010) Antibacterial and photocatalytic activities of sonochemically prepared ZnO and Ag–ZnO. J Alloys Compd 508: 587-591.
51. Zung L, Jiang L, Ding Y (2010) Investigation into antibacterial behaviour of suspensions of ZnO nanoparticles against *E. coli.* J Nanopart Res. 12:1625-1636.
52. http://www.omicsonline.org/scientific-reports/2157-7439-SR-557.pdf.